Journal of Power Sources 195 (2010) 5228–5234

Contents lists available at ScienceDirect

Journal of Power Sources

journal homepage: www.elsevier.com/locate/jpowsour

Improvement of water management in polymer electrolyte membrane fuel cell thanks to cathode cracks

Nicolas Karst[a,*], Vincent Faucheux[b], Audrey Martinent[b], Pierre Bouillon[a], Jean-Pierre Simonato[b,*]

[a] STMicroelectronics, Indre et Loire, 16 rue Pierre et Marie Curie, BP 7155, 37071 Tours Cedex 2, France
[b] Commissariat à l'Energie Atomique (CEA) LITEN-DTNM, 17 rue des Martyrs, 38054 Grenoble Cedex 9, France

ARTICLE INFO

Article history:
Received 30 October 2009
Received in revised form 12 February 2010
Accepted 6 March 2010
Available online 12 March 2010

Keywords:
Polymer electrolyte membrane fuel cell
Air breathing
Water management
Miniaturization
Liquid water removal
Water vizualization

ABSTRACT

The role of cathodic structure on water management was investigated for planar micro-air-breathing polymer electrolyte membrane fuel cells (PEMFCs). The electrical results demonstrate the possibility to decrease, with the same structure, both cell drying and cell flooding according to the environmental and operation conditions. Thanks to a simultaneous study of internal resistance and scanning electronic microscope (SEM) images, we demonstrate the advantageous influence of the presence of crack in cathodic catalytic layer on water management. On the one hand, the gold layer used as cathodic current collector is in contact with the electrolyte in the cracked zones which allows water maintenance within the electrolyte. It allows to decrease the cell drying and thus strongly increase the electrical performances. For cells operated in a 10% relative humidity atmosphere at 30 °C and at a potential of 0.5 V, the current density increases from 28 mA cm^{-2} to 188 mA cm^{-2} (+570%) for the cell with a cathodic cracked network. On the other hand, the reduction in oxygen barrier diffusion due to the cathodic cracks allows to improve oxygen diffusion. In flooding state, the current densities were higher for a cell with a cracked network. For cells operating in a 70% relative humidity atmosphere at 30 °C and at a potential of 0.2 V, a current density increase from 394 mA cm^{-2} to 456 mA cm^{-2} (16%) was noted for the cell with a cathodic cracked network. Microscopic observations allowed us to visualize water droplets growth mechanism in cathodic cracks. It was observed that the water comes out of the crack sides and partially saturates the cracks before emerging on cathodic collector. These results demonstrate that cathode structuration is a key parameter that plays a major role in the water management of PEMFCs.

1. Introduction

The new portable electronic devices require more and more energy densities for long term operation and the polymer electrolyte membrane fuel cell (PEMFC) appear to be an ideal candidate for this type of application [1]. However, in order to be compatible with wandering applications and competitive with the best Li-ion batteries currently available on the market it is necessary to miniaturize them [2–4]. Air-breathing fuel cells are considered particularly attractive for such applications because they use directly oxygen from air, which enables a significant decrease of the system complexity. Nevertheless, water management in air-breathing fuel cell has to take into account environmental variations such as relative humidity and temperature [5–8]. On the one hand, good cell hydration is necessary to ensure high electrical performances because proton conduction through the electrolyte depends directly on electrolyte hydration [9–11]. On the other hand, water excess leads to electrode flooding which lowers gas diffusion into the active part [12].

One of the most used device to manage at the same time drying and flooding cell is the control of gas humidity [13]. Büchi and Srinivasan observed that the electrical performance is 20–40% lower for a cell operated without gas humidification compared to operation with humidified gas [14]. However, such a system is too complex and too bulky to be integrated in portable applications. The addition of auxiliary has also been considered to evacuate water excess produced at the cathode. For instance, Buie et al. proposed to integrate an electroosmotic pump within the fuel cell [15]. With this pump, 19 mW is theoretically sufficient to evacuate all the water produced by a 1 cm^2 cell working at 1.0 A and 0.5 V, that is to say 5.6 μL min^{-1}. However, they observed experimentally that the power needed to evacuate such a water quantity was about three times larger and represented 15% of total fuel cell power production. They achieved potential more than three times larger (from 160 mV to 560 mV) for a flooding cell operated with an electroosmotic

* Corresponding authors. Tel.: +33 4 38 78 11 39; fax: +33 4 38 78 51 17.
E-mail addresses: nicolas.karst@gmail.com, nicolas.karst@grenoble-inp.fr (N. Karst), jean-pierre.simonato@cea.fr (J.-P. Simonato).

0378-7753/$ – see front matter © 2010 Elsevier B.V. All rights reserved.
doi:10.1016/j.jpowsour.2010.03.025

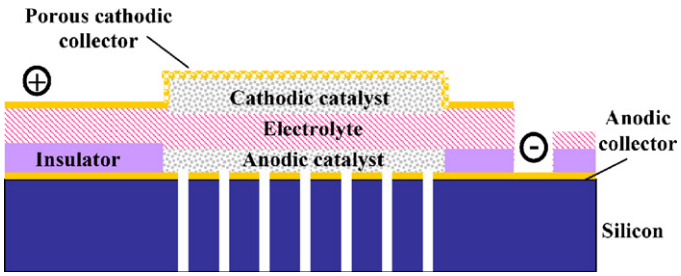

Fig. 1. Schematic cross-section of our micro-PEMFC.

pump. Such a system needs high potential to work (14 V) and requires a diagnostic tool to know when to start the pump, complicating strongly its integration in portable fuel cell. That is mainly why passive water management is desirable for this application. A passive solution commonly used to improve gas diffusion and to manage the cell flooding both on cathodic and anodic sides is the addition of a gas diffusion layer between the catalytic layers and the bipolar plates [16–19]. Watanabe et al. [16] showed that the electrical performance was four times higher for a cell with a gas diffusion layer, without any change concerning the catalytic layer. However, carbon type, porosity, quantity of hydrophobic polymer, wetting properties, thickness and manufacture technique of the gas diffusion layer are all key parameters influencing the electrical cell performances. A passive solution to avoid cell drying consists in the addition of platinum nanoparticles in the electrolyte [20,21]. Indeed, electrolyte gas permeability increases with polymer drying and the addition of platinum nanoparticles allows to produce water from the direct reaction between oxygen and hydrogen at the surface of these nanoparticles.

In this paper, we report on the influence of cathode structure on electrical performances and water management. Pictures were taken during cell operation in order to visualize cell flooding. A mechanism of water formation in cathode cracks based on optical observation is presented and overall improvement of air-breathing PEMFCs performances using structured cathode is demonstrated.

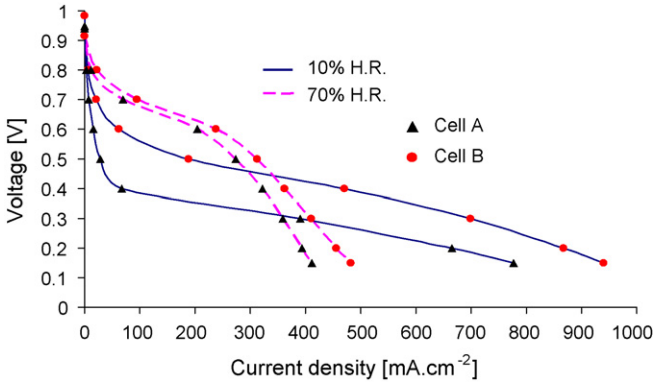

Fig. 3. Polarization curves for cell A (triangles) and cell B (circles) operated at 30 °C in an atmosphere at 10% of relative humidity (continued line) and 70% relative humidity (dashed line).

2. Experimental

Contrary to the traditional PEMFC structure, for which each component is separately manufactured before being assembled, our cell is obtained by successively depositing thin layers on a silicon pre-etched substrate, simply by using the chemical bounds between the different layers. This fabrication process avoids mechanical compression. A schematic cross-section of our micro-PEMFC is shown in Fig. 1. Detailed description of the structure is now added: the cathodic and anodic active layers were deposited by ink-jet printing techniques using an ink formulated with C/Pt (40 wt.% Pt on XC72 from Etek Inc.), electrolyte (1:1 Pt/Nafion ratio, DE521 Nafion solution from Ion Power Inc.) and various solvents such as iso-propanol, ethylene glycol and water. The adequate amounts of these solvents were adjusted in order to ensure a satisfactory dispersion of the particles and to obtain a viscosity of ca. 3 mPa s imposed by the ink-jet method. It was necessary to print several layers in order to obtain a sufficient thickness because the quantity of dry matter contained in the ink was lower than 5 wt.%.

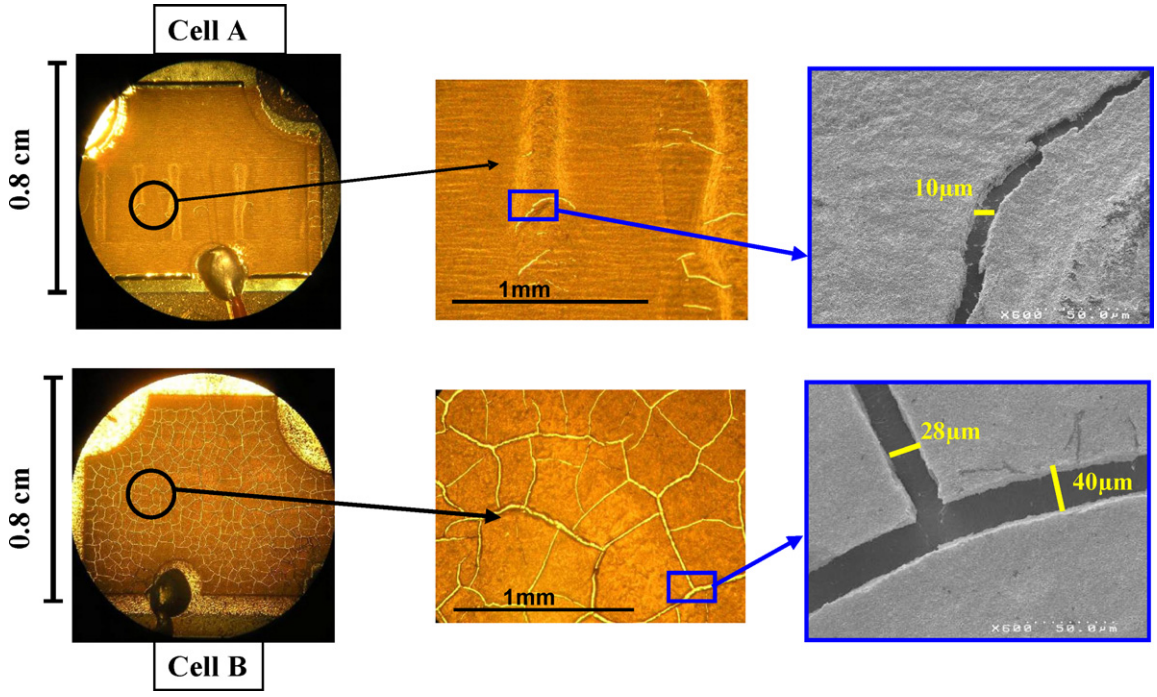

Fig. 2. Optical and SEM images of standard (cell A) and cracked (cell B) cathodes.

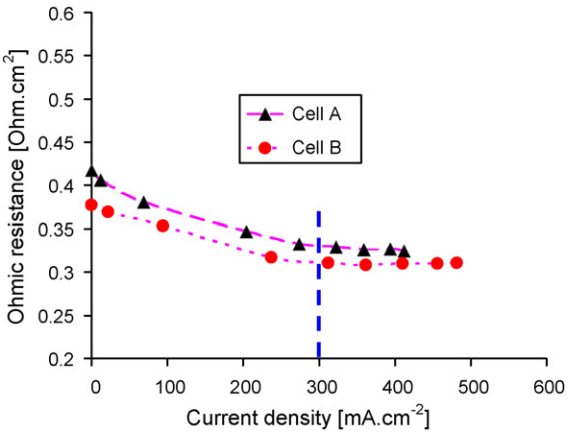

Fig. 4. Ohmic resistances extracted from impedance spectra for cell A (triangles) and cell B (circles) operated at 30 °C and 70% of relative humidity.

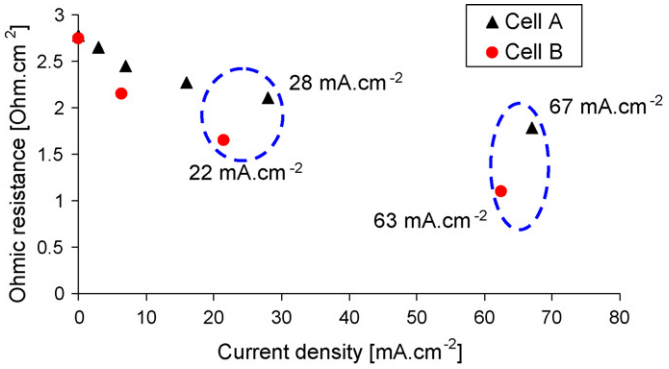

Fig. 5. Ohmic resistances extracted from impedance spectra for cell A (triangles) and cell B (circles) operated at 30 °C and 10% of relative humidity for current densities lower than 80 mA cm^{-2}.

The anode and the cathode were, respectively 10 μm and 20 μm thick. A 30 μm thick membrane was obtained by coating of a dispersion of D-2021 Nafion solution (from Dupont) on the anode. To complete the cell, a gold layer (0.5 μm) was deposited on the cathode. This layer was relatively thin in order to allow the diffusion of oxygen to the active layer [8].

In order to avoid variations of ambient conditions, a relative humidity generator (RH200, VTI Corporation) was connected through a heated line transfer to a 20 L incubator with adjustable temperature. The cell was then placed inside the incubator. To rapidly reach desired relative humidity, the flow of humidified air entering in the incubator was fixed at 5000 cm^3 min^{-1}.

The hydrogen flow used to feed the cell was controlled with Brooks Instruments flow meters (0.5–10.0 cm^3 min^{-1}).

The *I*–*V* curves and the AC impedance spectra were obtained using a multichannel potentiostat equipped with an impedance module (VMP3 from Bio-Logic SAS) in potentiostatic mode. A 10 mV amplitude sinusoidal signal was used and the frequencies were ranged from 100 kHz to 0.1 Hz.

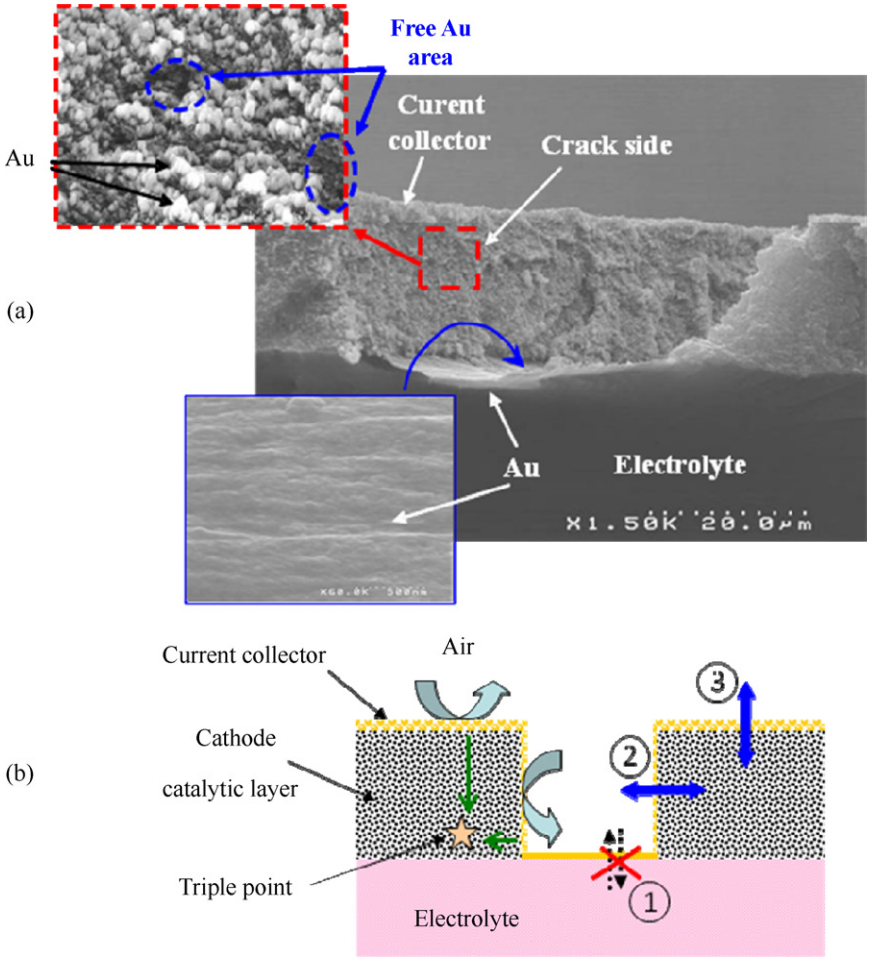

Fig. 6. (a) SEM crack images. (b) Schematic view of a crack.

The optical images were taken using a Leica DMLM microscope equipped with a DC300 camera. The scanning electron microscope (SEM) images were taken using a Hitachi S-4100 SEM.

3. Results and discussion

3.1. Influence of cathode structure on electrical performances

In order to study the cathode structure influence on water management, two different cathode deposit configurations were realized. As the quantity of dry matter contained in the ink is lower than 5%, it was necessary to print several layers in order to obtain a sufficient thickness. Thus, six layers were printed at the cathode while the substrate was maintained at 50 °C. In the first configuration, named herein cell A, the time between the deposit of two ink layers was more than 100 min. In the second configuration, named cell B, we reduced the time between two ink layer deposits to less than 2 min. After cathode fabrication, a 0.5 μm thick gold layer used as cathodic current collector was deposited by plasma-enhanced chemical vapour deposition (PECVD). Images of cells prepared in both configurations are presented in Fig. 2.

As shown on cell A cathode, only a few localized cracks were present. On the contrary, a large network of cracks can be observed on cell B cathode. From optical images analysis, we estimated that the surface occupied by the cracks on cell B corresponded to approximately 8% of the cell active surface. The cracks widths measured by SEM were between 10 μm and 60 μm. In order, to evaluate the influence of cracks on electrical performances and water management, polarization curves were realized for each cell in controlled atmosphere. Once the desired relative humidity was reached in the test chamber, the cell was left at open circuit voltage (OCV) for 3 h in order to stabilize membrane hydration [10,22] and then a range of voltages (from 0.8 V to 0.15 V) was imposed to the cell. The resulting current density was read after 30 min of operation and an impedance spectrum was then recorded. It should be noted that after every 30 min cycle the cell was stabilized at OCV for 15 min in order to remove water excess at the cathode. A hydrogen flow of 8.5 $cm^3\ min^{-1}$ was supplied to the cell. The polarization curves obtained for each cell operated in 10% and 70% relative humidity atmospheres at 30 °C are presented in Fig. 3.

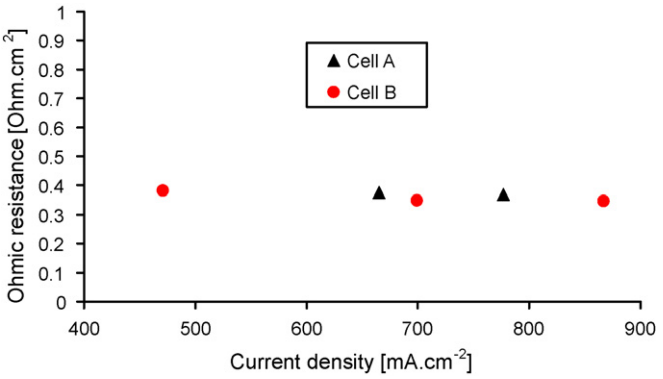

Fig. 7. Ohmic resistances extracted from impedance spectra for cell A (triangles) and cell B (circles) operated at 30 °C and 10% of relative humidity for current densities higher than 400 mA cm^{-2}.

It can be noted that the electrical performances of cell B were higher than that of cell A, and the lower the relative humidity, the higher the differences between the two cell performances. In order to observe the influence of the cracks on ohmic resistance, it was necessary to minimize the ohmic losses due to the electrolyte and electrode drying. Thus we only considered the resistance values obtained when the electrolyte was well hydrated, i.e. when the cells were operated in a 70% relative humidity atmosphere at current densities higher than 300 mA cm^{-2}. Ohmic resistance values were extracted from impedance spectra at the intersection point at high frequencies between the *x*-axis and the Nyquist plot [23,24]. As presented in Fig. 4, under these conditions the ohmic resistance value was stable in spite of current density increase and water production enhancement, confirming that the electrolyte was saturated with water. The ohmic resistance deviation observed between the two cells is not significant (<0.02 Ω cm^2), thus it seems reasonable to assume that the presence of cracks does not influence the ohmic resistance.

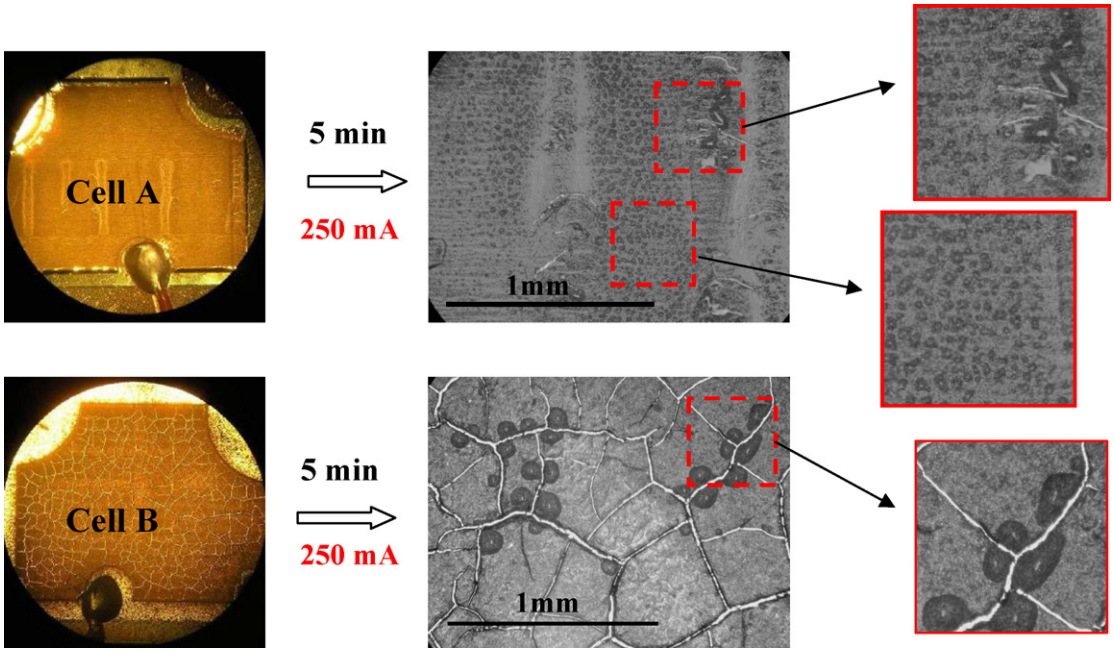

Fig. 8. Water observation on cathodic collector surfaces for cell A (up) and cell B (down) operated at 250 mA.

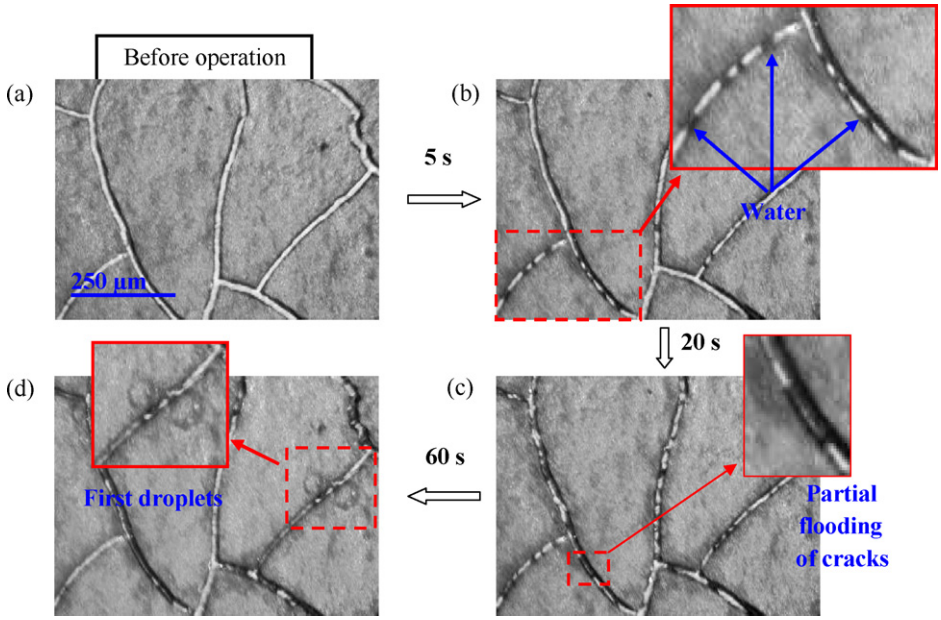

Fig. 9. (a) Image of cell B cathodic collector before cell operation. Observation of water evolution on cathodic collector surface for cell B operated at 250 mA after (b) 5 s, (c) 20 s and (d) 60 s.

3.2. Influence of cathode structure on oxygen and water management

In order to understand why the electrical performances were different, we plotted the data obtained at current densities lower than 80 mA cm^{-2} for cells operated at 10% relative humidity. As shown in Fig. 5, although current densities (marked with a dotted blue circle) and water generation were almost similar, the ohmic resistance values were lower for cell B when compared to cell A.

To explain this significant difference, we performed SEM observations on cell B as presented in Fig. 6. First we can see on SEM images the presence of a dense gold layer on the electrolyte. This point was confirmed by X-ray microanalysis using a SEM Philips XL 30 equipped with an energy dispersion electronic detector (EDS). During ink drying, cracks were formed through the whole thickness of the catalytic layer, allowing direct contact of the current collector with the electrolyte. A crack is schematically represented in Fig. 6(b). The fact that the gold layer was dense and continuous prevented any water transfer (way 1). Therefore, we suggest that the low ohmic resistance observed previously (Fig. 5) for cell B at low current densities was mainly due to the water containment within the electrolyte because of the waterproof gold layer pres-

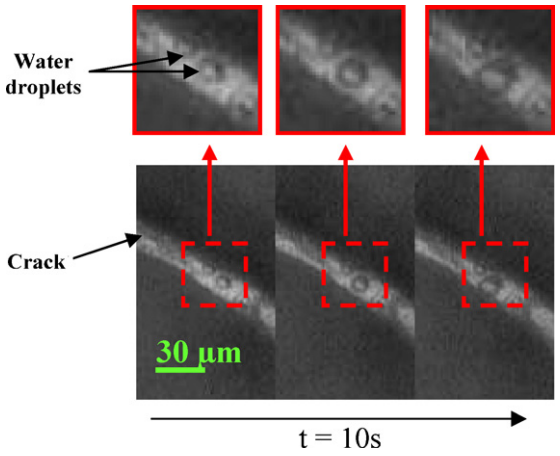

Fig. 11. Water droplets formation on crack centre for cell B operated at 250 mA.

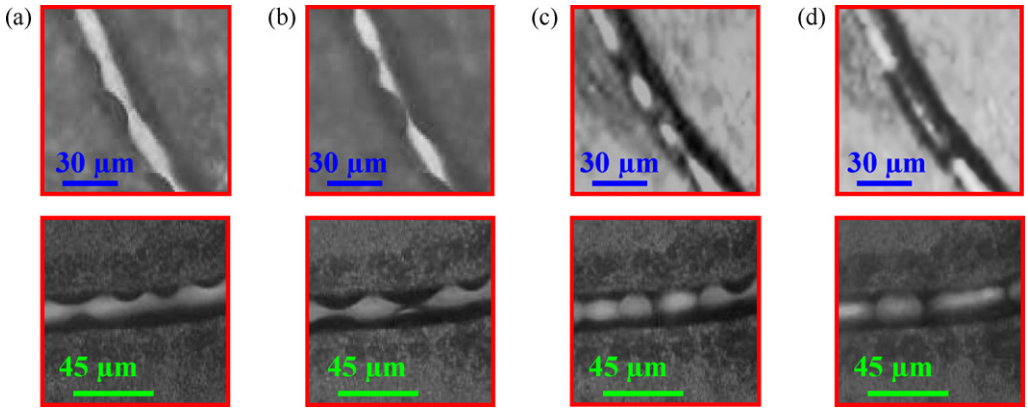

Fig. 10. Observation of water growth mechanism in two different cracks for a cell B operated at 250 mA. (a) Appearance of water droplets on crack sides, (b) growth of droplets, (c) collapsing of droplets and (d) formation of water domains.

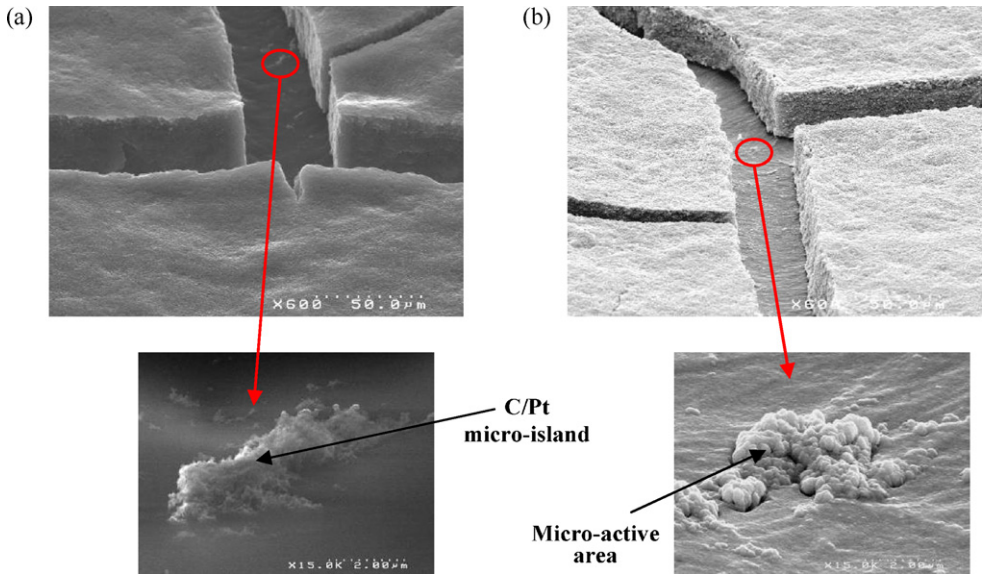

Fig. 12. SEM images before (a) and after (b) gold deposit showing the presence of micro-active areas within the cracks for cell B.

ence. The surface occupied by these strips was lower than 10% of the overall surface, but even small amount of water can explain the differences observed in ohmic resistance values between the two cells since electrolyte conductivity strongly evolved with water content [9].

The data obtained at 10% relative humidity for current densities higher than 400 mA cm^{-2} are presented in Fig. 7. The ohmic resistance was stable at ca. 0.35 Ω cm^2 confirming that the electrolyte was saturated with water and that electrodes were well hydrated in both cases. Therefore, the assumption suggested previously concerning the water containment in electrolyte was not sufficient anymore to explain the differences observed at high current densities. A SEM image from the side of a crack is presented in Fig. 6(a). It shows the presence of a discontinuous gold layer along the sidewalls with catalytic areas of several squared micrometers in direct contact with oxygen from air (way 2). Thus, as depicted in Fig. 6(b) the diffusion barrier was weaker, the mean path to reach some triple points was reduced (for cell A, oxygen could only penetrate in the active layer by the way 3), and in addition the presence of cracks increased the overall specific surface when compared to cell A. The presence of the cracks allowed an improvement of oxygen diffusion to the active layer.

In order to visualize the influence of cathode structure on water formation, the A and B cells under operation were placed under the microscope. Fogging of the microscope objective was mitigated by an anti-fog coating. The cells' operating temperature and ambient relative humidity were, respectively 25 °C and 50%. The two cells were operated in a flooding state at a current of 250 mA. The images presented in Fig. 8 were taken after 5 min of operation. Cell A images show that on the one hand, water forms low diameter droplets on the whole surface of the cathodic collector, and on the other hand larger water droplets appear near the cracks. The numerous droplets spread all over the surface strongly reduce the oxygen access to the active layer, involving an important cell flooding. Concerning cell B, we noted that water appears preferentially near the cracks in the form of large diameters drops. It implies that only some localized areas become impermeable to oxygen, allowing a gas free access on a more important surface than for cell A.

A further insight into water formation mechanisms for a cell with cracks was carried out using an optical microscope during cell operation. A first image was taken before cell operation as shown in Fig. 9(a). After 5 s (Fig. 9(b)), water (dark marks) appeared in the cracks. The quantity of water present in the cracks increased as a function of time, leading to the partial saturation of channels (Fig. 9(c)) before emergence on cathodic collector surface (Fig. 9(d)).

As presented in Fig. 10, a zoom was achieved on two cracks in order to observe the appearance of liquid water. We noted that the mechanism was independent of the crack size. Indeed, we first observed the appearance of water droplets on crack sides (Fig. 10(a)) whose volume gradually increased (Fig. 10(b)). Once a critical size was reached, these droplets went in contact with the opposite wall or with droplets coming from the opposite side (Fig. 10(c)) and formed micrometric water domains within cracks through coalescing of droplets (Fig. 10(d)).

Another phenomenon was pointed out during water formation observations within the cracks. Indeed, as presented in Fig. 11 we noted sometimes the formation of water droplets in the middle of a crack. However, we presented previously the cracks as being non-active zones.

Actually, during the active layer split, some tiny fractions remained fixed to the electrolyte constituting active micro-areas, as depicted in Fig. 12. Indeed, before gold layer deposit, C/Pt micro-islands were in contact with Nafion within the cracks (Fig. 12(a)) and become active zones after gold deposit (Fig. 12(b)). Nevertheless, the amount of water generated by these micro-zones is negligible compared to the total water generated by the cell due to the scarce presence of these minute catalytic domains.

4. Conclusion

The effect of cathode structure on electrical performances and on water management in air-breathing micro-PEMFC was experimentally investigated. We have demonstrated that the performances of a cell presenting a crack network are higher than those obtained for a standard cell. Indeed, for cells operating in a 10% relative humidity atmosphere at 30 °C and at a potential of 0.5 V, the current density was increased from 28 mA cm^{-2} to 188 mA cm^{-2} (+570%) when a network of cracks was present. However, between the two kinds of cell, the performance differences decrease with relative humidity increase: a profit of 14% (from 204 mA cm^{-2} to 237 mA cm^{-2}) was observed for a cathode cracked cell functioning

in a 70% relative humidity atmosphere at 30 °C and for a tension of 0.5 V. Thanks to simultaneous electrical data (*I–V*, ohmic resistance) and high resolution images, we managed to explain the observed differences of electrical performances. Indeed, the presence in the crack bottoms of a gold layer on the electrolyte allows water containment when the cell is in drying condition. Moreover, the oxygen diffusion barrier is less important on the side of the cracks and the mean path to reach a triple point was reduced for a cell with cracked cathode. Thus, the cracks allow an improvement of oxygen diffusion towards the cathode catalytic sites. The water produced at the cathode for an operating cell was observed by using an optical microscope. This allowed us to point out the water discharge differences between a cracked and a standard cell. Indeed, we showed for a cracked cell that water leaves preferentially near the cracks whereas for a standard cell the water leaves on the whole cathodic collector, strongly reducing the oxygen diffusion to the active sites. Observations at higher resolution allowed us to identify the water drop growth mechanism within the cracks. Control of major factors influencing the generation and structure of cracks is currently under study. We think that these observations will be helpful for significant improvements in water management, and cathode structuration will have to be considered in depth in conjunction with potential auxiliaries.

References

[1] C.K. Dyer, J. Power Sources 106 (2002) 31–34.
[2] J.S. Wainright, R.F. Savinell, C.C. Liu, M. Litt, Electrochim. Acta 48 (2003) 2869–2877.
[3] S.J. Lee, Y.M. Lee, C.Y. Lee, J.J. Lai, F.H. Kuan, C.W. Chuang, J. Power Sources 171 (2007) 148–154.
[4] J.P. Meyers, H.L. Maynard, J. Power Sources 109 (2002) 76–88.
[5] T. Hottinen, M. Noponen, T. Mennola, O. Himanen, M. Mikkola, P. Lund, J. Appl. Electrochem. 33 (2003) 265–271.
[6] T. Fabian, J.D. Posner, R. O'Hayre, S.W. Cha, J.K. Eaton, F.B. Prinz, J.G. Santiago, J. Power Sources 161 (2006) 168–182.
[7] M.M. Saleh, T. Okajima, M. Hayase, F. Kitamura, T. Ohsaka, J. Power Sources 164 (2007) 503–509.
[8] N. Karst, V. Faucheux, A. Martinent, P. Bouillon, J.Y. Laurent, F. Druart, J.P. Simonato, J. Power Sources 195 (2010) 1156–1162.
[9] T.E. Springer, T.A. Zawodzinski, S. Gottesfeld, J. Electrochem. Soc. 138 (1991) 2334–2341.
[10] Y. Sone, P. Ekdunge, D. Simonsson, J. Electrochem. Soc. 143 (1996) 1254–1259.
[11] C. Yang, P. Costamagna, S. Srinivasan, J. Benziger, A.B. Bocarsly, J. Power Sources 103 (2001) 1–9.
[12] J. Chen, T. Matsuura, M. Hori, J. Power Sources 131 (2004) 155–161.
[13] J. Larminie, A. Dicks, Fuel Cell System Explained, 1st ed., John Wiley & Sons, 2000.
[14] F.N. Büchi, S. Srinivasan, J. Electrochem. Soc. 144 (1997) 2767–2772.
[15] C.R. Buie, J.D. Posner, T. Fabian, S.W. Cha, D. Kim, F.B. Prinz, J.K. Eaton, J.G. Santiago, J. Power Sources 161 (2006) 191–202.
[16] M. Watanabe, M. Tomikawa, S. Motoo, J. Electroanal. Chem. 182 (1985) 193–196.
[17] E. Passalacqua, G. Squadrito, F. Lufrano, A. Patti, L. Giorgi, J. Appl. Electrochem. 31 (2001) 449–454.
[18] Y. Bultel, K. Wiezell, F. Jaouen, P. Ozil, G. Lindbergh, Electrochim. Acta 51 (2005) 474–488.
[19] S. Park, J.W. Lee, B.N. Popov, J. Power Sources 177 (2008) 457–463.
[20] M. Watanabe, H. Uchida, M. Emori, J. Electrochem. Soc. 145 (1998) 1137–1141.
[21] X. Zhu, H. Zhang, Y. Zhang, Y. Liang, X. Wang, B. Yi, J. Phys. Chem. B 110 (2006) 14240–14248.
[22] D.J. Burnett, A.R. Garcia, F. Thielmann, J. Power Sources 160 (2006) 426–430.
[23] S.S. Hsieh, S.H. Yang, C.L. Feng, J. Power Sources 162 (2006) 262–270.
[24] W.H. Zhu, R.U. Payne, B.J. Tatarchuk, J. Power Sources 168 (2007) 211–217.